Appendix F
Subcarrier and Symbol-Loop SNR Performance

F.1 Subcarrier I- and IQ-Loops

Compared to the conventional subcarrier loop (unmodified), which employs the I-arm as shown in Fig. F-1, the modified subcarrier loop, depicted in Fig. F-2, utilizes both the I- and Q-arms of the baseband signal for tracking. The loop SNRs for both schemes are derived here and compared to the case when the carrier is locked. For CSC, the I- and Q-channels at the input of the subcarrier loop are respectively given as

$$\begin{aligned} I(t_i) &= \sqrt{P}d(t_i)Sqr\left(\Delta\omega_{sc}t_i + \theta_{sc}\right)\cos(\Delta\omega_c t_i) + n_I(t_i) \\ Q(t_i) &= \sqrt{P}d(t_i)Sqr\left(\Delta\omega_{sc}t_i + \theta_{sc}\right)\sin(\Delta\omega_c t_i) + n_Q(t_i) \end{aligned} \tag{F-1}$$

where $n_I(t_i)$ and $n_Q(t_i)$ are independent Gaussian noise processes and all other parameters were previously defined. As shown in Fig. F-2, both the I- and Q-components are multiplied by the square-wave references and averaged over one symbol period (assuming perfect symbol synchronization), resulting in [1]

$$\begin{aligned} I_s(k) &= \sqrt{P}d(k)\,f(\phi_{sc})\cos(\Delta\omega_c t_k) + n_{I\,s}(k) \\ I_c(k) &= \sqrt{P}d(k)\,g(\phi_{sc})\cos(\Delta\omega_c t_k) + n_{I\,c}(k) \\ Q_s(k) &= \sqrt{P}d(k)\,f(\phi_{sc})\sin(\Delta\omega_c t_k) + n_{I\,s}(k) \\ Q_c(k) &= \sqrt{P}d(k)\,g(\phi_{sc})\sin(\Delta\omega_c t_k) + n_{I\,c}(k) \end{aligned} \tag{F-2}$$

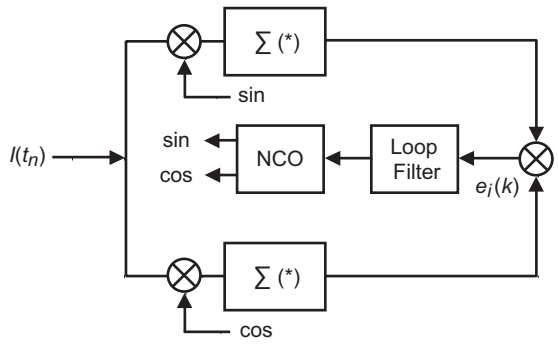

Fig. F-1. The unmodified subcarrier loop.

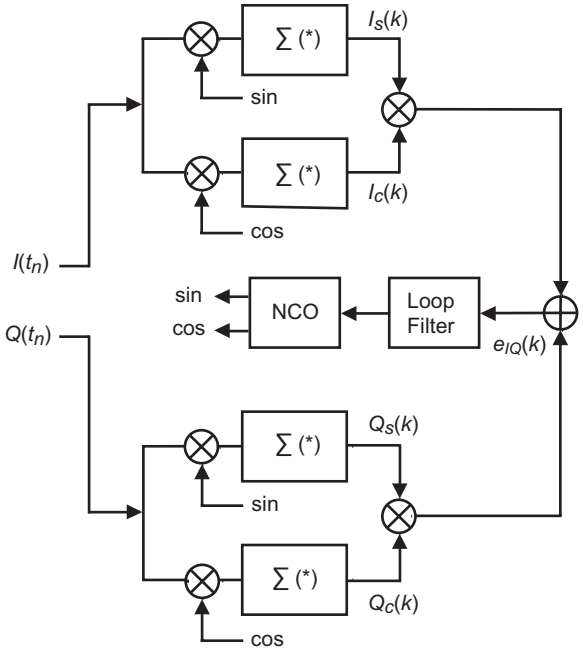

Fig. F-2. The modified subcarrier loop.

where k denotes the symbol index, $f(\phi_{sc}) = \left(1 - 2\,|\,\phi_{sc}\,|/\pi\right)$ for $|\,\phi_{sc}\,| \le \pi$, $g(\phi_{sc}) = 2\phi_{sc}/\pi$ for $|\,\phi_{sc}\,| \le \pi\, w_{sc}\,/\,2|, Var\left[n_{Is}(k)\right] = Var\left[n_{Ic}(k)\right] = Var\left[n_{Qs}(k)\right]$ $= \sigma_n^2 = N_0/2T_s$. The error signal of the conventional and modified subcarrier loops, respectively, are given as

$$\begin{aligned} e(k)_I &= P\, f(\phi_{sc})\, g(\phi_{sc}) \cos^2(\Delta\omega_c t_k) + N_I(k) \\ e(k)_{IQ} &= P\, f(\phi_{sc})\, g(\phi_{sc}) + N_{IQ}(k \end{aligned} \tag{F-3}$$

where the variances of the noise terms, respectively (after averaging over $\Delta\omega_c t_k$, assuming uniform distribution), are given as

$$\begin{aligned}\sigma^2_{N_{IQ}} &= P\sigma_n^2 + 2\sigma_n^4 \\ \sigma^2_{N_I} &= P\sigma_n^2/2 + \sigma_n^4\end{aligned} \tag{F-4}$$

The slope of the phase detector response curve can now be found by taking the first derivative of the average error signal with respect to ϕ_{sc}, and afterwards setting $\phi_{sc} = 0$. Accordingly, the slopes of the conventional and modified subcarrier loops are given as

$$\begin{aligned}K^I_{g\,sc} &= \frac{1}{\pi}P \\ K^{IQ}_{g\,sc} &= \frac{2}{\pi}P\end{aligned} \tag{F-5}$$

Note the slope of the IQ-arm is identical to the slope of the I-arm when the carrier is locked [1]. Assuming linear theory, the loop SNR for the subcarrier loop is given as

$$\rho_{sc} = \frac{1}{2B_{sc}T_s}\frac{K_g^2}{\sigma_N^2} \tag{F-6}$$

where B_{sc} is the one-sided noise bandwidth of the loop. Simplifying, the I- and IQ-arm loop SNRs are respectively given as

$$\begin{aligned}\rho^I_{sc} &= \left(\frac{2}{\pi}\right)^2 \frac{P/N_0}{2B_{sc}\,w_{sc}}\left(1 + \frac{1}{PT_s/N_0}\right)^{-1} \\ \rho^{IQ}_{sc} &= \left(\frac{2}{\pi}\right)^2 \frac{P/N_0}{B_{sc}\,w_{sc}}\left(1 + \frac{1}{PT_s/N_0}\right)^{-1}\end{aligned} \tag{F-7}$$

For comparison, the I-arm loop SNR when the carrier is locked is given in Eq. (5.2-7). Figure F-3 illustrates the subcarrier-loop SNRs when the I-arm, IQ-arm, and the I-arm with the carrier locked are used. For low symbol SNRs, the I-arm has a loop SNR that is 6 dB lower than the case when the carrier is locked. Using the IQ-arm, however, recovers 3 dB of the 6 dB but at the expense of more hardware. At high symbol SNRs, the performance of the IQ-arm is identical to that of the I-arm when the carrier is locked.

The behavior of the I-arm and IQ-arm for the subcarrier loop is investigated when the carrier is actually locked. For the I-arm, the subcarrier is normalized by a slope that is less than the actual operating slope. Consequently, the

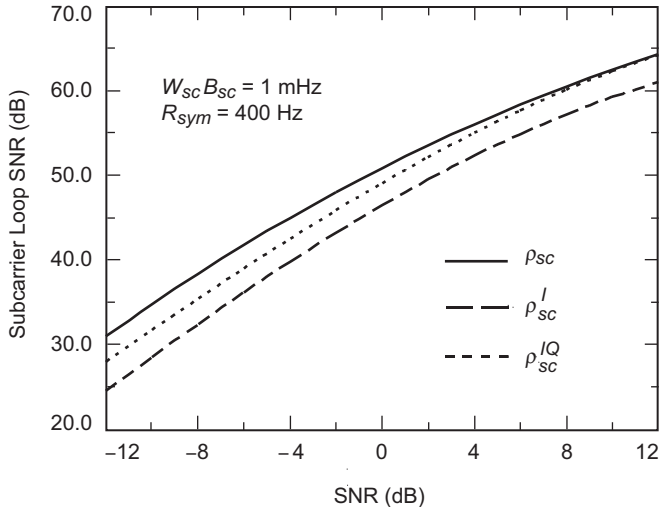

Fig. F-3. Subcarrier-loop SNR versus symbol SNR.

operating bandwidth of the loop is actually narrower that the one specified. Fortunately, for the IQ arm, the subcarrier is normalized by the correct slope.

F.2 Digital Data-Transition Tracking I- and IQ-Loops

Similar to the subcarrier loop, the conventional digital data-transition tracking loop (DTTL) shown in Fig. F-4 will be modified to utilize both the I- and Q-channels, as depicted in Fig. F-5. Assuming perfect subcarrier demodulation, the I- and Q-components for CSC are given as

$$\begin{aligned} I_k &= \sqrt{P}\, d_k \cos(\phi_c) + n_k^I \\ Q_k &= \sqrt{P}\, d_k \sin(\phi_c) + n_k^Q \end{aligned} \tag{F-8}$$

where n_k^I and n_k^Q are independent Gaussian random variables with variance $\sigma_n^2 = N_0/2T$ and $\phi_c = 2\pi\Delta f_c\, t + \theta_c$ is the difference between the predicted and actual IF carrier frequency.

The performance of the DTTL has been derived in [2] assuming the carrier is locked $(\phi_c = 0)$. When this is not the case, as in CSC, the loop suffers degradation, and the objective here is to quantify the decrease in performance for both the conventional and the modified DTTL. The analysis of the DTTL follows closely that of [2] with the difference now being that the data are modulated by a slowly varying cosine function. Assuming the equivalent mathematical model of the DTTL in terms of a phase-locked loop (PLL), all the relevant parameters (slope of the S-curve and normalized equivalent noise spectrum) are derived conditioned on ϕ_c. Afterwards, these parameters are averaged over ϕ_c, assuming ϕ_c is uniformly distributed from $-\pi$ to π.

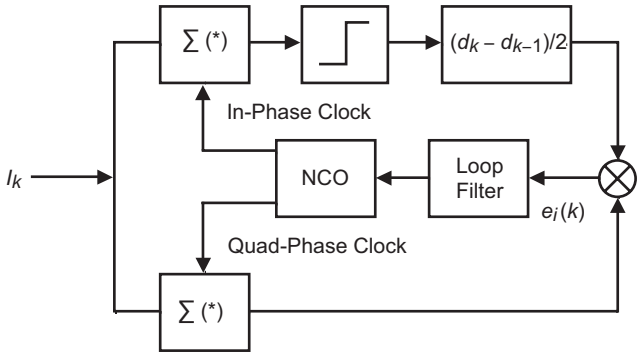

Fig. F-4. The unmodified digital DTTL.

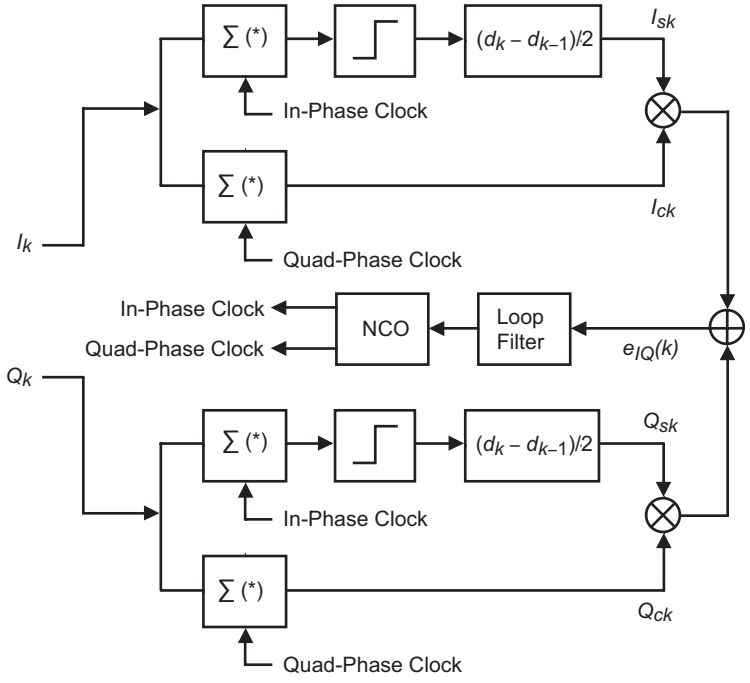

Fig. F-5. The modified digital DTTL.

The normalized mean of the error signal, e_k, conditioned on the normalized timing error, λ (in cycles), and the carrier predict error, ϕ_c, is the normalized phase detector characteristic $g_n(\lambda, \phi_c)$, commonly termed the loop S-curve. Following steps similar to those in [2], $g_n^I(\lambda, \phi_c)$ and $g_n^{IQ}(\lambda, \phi_c)$, the S-curves of the conventional and the modified DTTL, are respectively given as

$$
\begin{aligned}
g_n^I(\lambda,\phi_c) &= \lambda\left|\cos(\phi_c)\right|\mathrm{erf}(B) - \frac{w_{sy}-2\lambda}{8}\left|\cos(\phi_c)\right|\left[\mathrm{erf}(A)-\mathrm{erf}(B)\right] \\
g_n^{IQ}(\lambda,\phi_c) &= \lambda\left|\cos(\phi_c)\right|\mathrm{erf}(B) + \lambda\left|\sin(\phi_c)\right|\mathrm{erf}(B') \\
&\quad - \frac{w_{sy}-2\lambda}{8}\left|\cos(\phi_c)\right|\left[\mathrm{erf}(A)-\mathrm{erf}(B)\right] \\
&\quad - \frac{w_{sy}-2\lambda}{8}\left|\sin(\phi_c)\right|\left[\mathrm{erf}(A')-\mathrm{erf}(B')\right]
\end{aligned}
\tag{F-9}
$$

where
$A = \sqrt{E_s/N_0}\left|\cos(\phi_c)\right|$, $A' = \sqrt{E_s/N_0}\left|\sin(\phi_c)\right|$, $B = \sqrt{E_s/N_0}\,(1-2\lambda)\left|\cos(\phi_c)\right|$, and $B' = \sqrt{E_s/N_0}\,(1-2\lambda)\left|\sin(\phi_c)\right|$. To compute the S-curve conditioned only on λ, $g_n^I(\lambda,\phi_c)$ and $g_n^{IQ}(\lambda,\phi_c)$ are numerically integrated over ϕ_c, assuming uniform distribution. Setting ϕ_c to zero in Eq. (F-9) results in the same S-curve as in [2].

The first derivative of the S-curve at $\lambda = 0$ is given as

$$
\begin{aligned}
K_{g,sy}^I(\phi_c) &= \left|\cos(\phi_c)\right|\mathrm{erf}(A) - \frac{w_{sy}}{2}\cos^2(\phi_c)\sqrt{\frac{E_s}{N_0\pi}}\,e^{-A^2} \\
K_{g,sy}^{IQ}(\phi_c) &= \left|\cos(\phi_c)\right|\mathrm{erf}(A) - \frac{w_{sy}}{2}\cos^2(\phi_c)\sqrt{\frac{E_s}{N_0\pi}}\,e^{-A^2} \\
&\quad + \left|\sin(\phi_c)\right|\mathrm{erf}(A') - \frac{w_{sy}}{2}\sin^2(\phi_c)\sqrt{\frac{E_s}{N_0\pi}}\,e^{-A'^2}
\end{aligned}
\tag{F-10}
$$

where $K_{g,sy}^I(\phi_c)$ and $K_{g,sy}^{IQ}(\phi_c)$ denote the slope of the S-curve for the conventional and modified DTTLs, respectively, conditioned on ϕ_c. Numerically integrating over the carrier phase, ϕ_c, results in the unconditional slopes, respectively denoted $K_{g,sy}^I$ and $K_{g,sy}^{IQ}$. Setting ϕ_c in Eq. (F-10) to zero results in

$$
K_{g,sy} = \mathrm{erf}\left(\sqrt{\frac{E_s}{N_0}}\right) - \frac{w_{sy}}{2}\sqrt{\frac{E_s}{N_0\pi}}\,e^{-E_s/N_0} \tag{F-11}
$$

which is identical to the slope given in [2]. Figure F-6 lists the ratio of $K_{g,sy}^I / K_{g,sy}$ and $K_{g,sy}^{IQ} / K_{g,sy}$ for different symbol SNRs and window sizes. At low symbol SNR, $K_{g,sy}$ and $K_{g,sy}^{IQ}$ are about the same, while $K_{g,sy}^I$ is about twice as large.

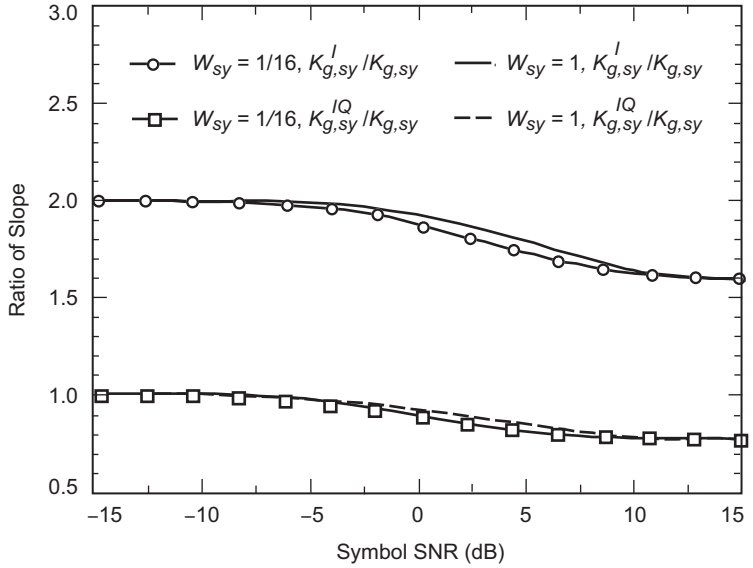

Fig. F-6. DTTL symbol versus ratio of slope.

Also, the normalized noise spectrum at $\lambda = 0$ can be shown to be

$$h^{I}(0,\phi_c) = 1 + 0.5\,w_{sy}\frac{E_s}{N_0}\cos^2(\phi_c) - \frac{w_{sy}}{2}\left[\frac{1}{\sqrt{\pi}}e^{-A^2} + \sqrt{\frac{E_s}{N_0}}\left|\cos(\phi_c)\right|\mathrm{erf}(A)\right]^2$$

$$h^{IQ}(0,\phi_c) = 2 + 0.5\,w_{sy}\frac{E_s}{N_0} - \frac{w_{sy}}{2}\left[\frac{1}{\sqrt{\pi}}e^{-A^2} + \sqrt{\frac{E_s}{N_0}}\left|\cos(\phi_c)\right|\mathrm{erf}(A)\right]^2$$

$$- \frac{w_{sy}}{2}\left[\frac{1}{\sqrt{\pi}}e^{-A'^2} + \sqrt{\frac{E_s}{N_0}}\left|\sin(\phi_c)\right|\mathrm{erf}(A')\right] \qquad \text{(F-12)}$$

where $h^{I}(0,\phi_c)$ and $h^{IQ}(0,\phi_c)$ denote the normalized noise spectra for the conventional and modified DTTLs, respectively, conditioned on ϕ_c. Numerically integrating over the carrier phase, ϕ_c, results in the unconditional normalized noise spectra, respectively denoted as $h^{I}(0)$ and $h^{IQ}(0)$. Setting ϕ_c in Eq. (F-12) to zero results in

$$h^{I}(0) = 1 + 0.5\,w_{sy}\frac{E_s}{N_0} - \frac{w_{sy}}{2}\left[\frac{1}{\sqrt{\pi}}e^{-E_s/N_0} + \sqrt{R_s}\,\mathrm{erf}\left(\sqrt{\frac{E_s}{N_0}}\right)\right]^2 \qquad \text{(F-13)}$$

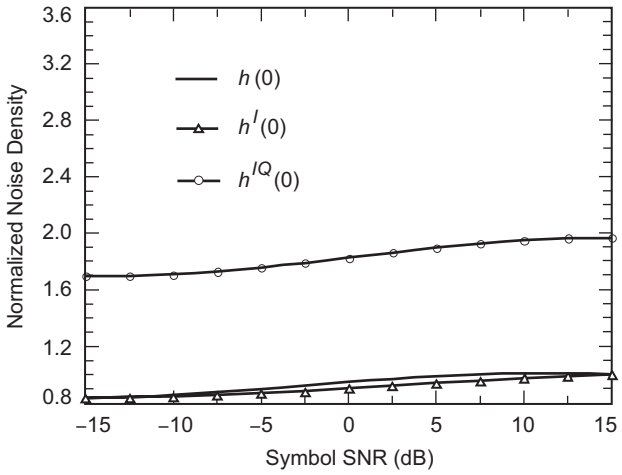

Fig. F-7. DTTL symbol SNR versus normalized noise density.

which is the same as the normalized noise spectrum given in [2]. Figure F-7 lists values of $h(0)$, $h^I(0)$, and $h^{IQ}(0)$ for different symbol SNRs at $w_{sy} = 1$. It is evident that $h(0)$ is slightly greater than $h^{IQ}(0)$ but significantly less than $h^I(0)$.

Assuming linear theory, the loop SNR for the DTTL is given as

$$\rho_{sy} = \frac{1}{2\pi^2} \frac{P}{N_0 w_{sy} B_{sy}} \mathrm{L} \tag{F-14}$$

where $\mathrm{L} = K_{g,sy}^2 \big/ h(0)$. Furthermore, the loop SNRs for the conventional and modified DTTLs, denoted ρ_{sy}^I and ρ_{sy}^{IQ}, are found by normalizing Eq. (F-14) by $\mathrm{L}^I = (K_{g,sy}^I)^2 \big/ h^I(0)$ or $\mathrm{L}^{IQ} = (K_{g,sy}^{IQ})^2 \big/ h^{IQ}(0)$, respectively. Figure F-8 illustrates the loop SNR of the DTTL using the I-arm, IQ-arm, and I-arm when the carrier is locked. At low symbol SNR, it is clear that using only the I-arm reduces the loop SNR by 6 dB as compared to the case when the carrier is locked, and that utilizing the IQ-arm recovers 3 dB of the 6 dB.

The behavior of the I- and IQ-arms for the symbol loop is investigated when the carrier is actually locked. For the I-arm, the symbol loop is normalized by a slope that is less than the actual operating slope, as shown in Fig. F-6. Consequently, the operating bandwidth of the loop is actually narrower than the one specified. Fortunately, for the IQ-arm at a low symbol SNR, the symbol loop is normalized by the correct slope. For a high symbol SNR, however, the symbol loop for the IQ-arm is normalized by a slope that is greater than the actual operating slope. Consequently, the operating bandwidth of the loop is actually wider than the one specified.

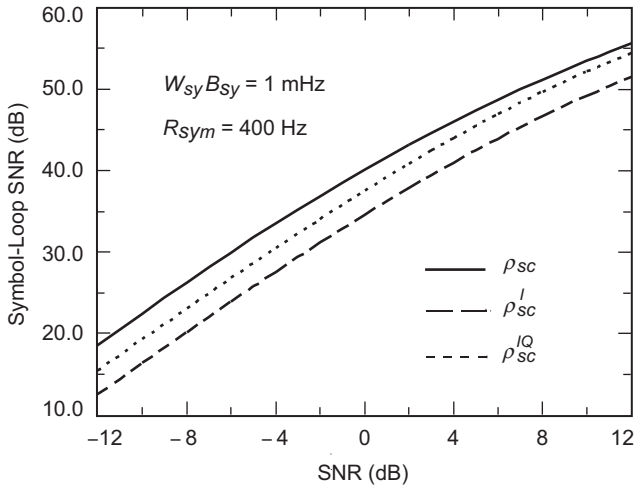

Fig. F-8. Symbol-loop SNR versus symbol SNR.

References

[1] W. J. Hurd and S. Aguirre, "A Method to Dramatically Improve Subcarrier Tracking," *The Telecommunications and Data Acquisition Progress Report 42-86, April–June 1986*, Jet Propulsion Laboratory, Pasadena, California, pp. 103–110, August 15, 1986. http://ipnpr.jpl.gov/progress_report/

[2] M. K. Simon, "Analysis of the Steady State Phase Noise Performance of a Digital Data-Transition Tracking Loop," *Space Programs Summary 37-55*, Jet Propulsion Laboratory, Pasadena, California, vol. 3, pp. 54–62, February 1969.